# Fluorescence exclusion: a rapid, accurate and powerful method for measuring yeast cell volume

Daniel García-Ruano[1], Larisa Venkova[2, 3], Akanksha Jain[1], Joseph C. Ryan[1], Vasanthakrishnan Radhakrishnan Balasubramaniam[1], Matthieu Piel[2] and Damien Coudreuse[1, 3, *]

[1] Institute of Genetics and Development of Rennes, UMR 6290, CNRS – University of Rennes 1, France

[2] Institut Curie and Institut Pierre Gilles de Gennes, PSL Research University, CNRS UMR 144, Paris, France.

[3] Institute of Biochemistry and Cellular Genetics, CNRS UMR 5095, Bordeaux, France

[*] Corresponding author: damien.coudreuse@ibgc.cnrs.fr

*Running title:* Measuring yeast cell volume

*Keywords*: Cell volume, yeast, fluorescence exclusion

## SUMMARY STATEMENT

Fluorescence exclusion provides a powerful method to accurately measure the volume of yeast cells at both the population and single-cell levels.


## ABSTRACT

Cells exist in an astonishing range of volumes across and within species. However, our understanding of cell size control remains limited, due in large part to the challenges associated with accurate determination of cell volume. Much of our comprehension of size regulation derives from yeast models, but even for these morphologically stereotypical cells, assessment of cell volume has mostly relied on proxies and extrapolations from two-dimensional measurements. Recently, the fluorescence exclusion method (FXm) was developed to evaluate the size of mammalian cells, but whether it could be applied to smaller cells remained unknown. Using specifically designed microfluidic chips and an improved data analysis pipeline, we show here that FXm reliably detects subtle differences in the volume of fission yeast cells, even for those with altered shapes. Moreover, it allows for the monitoring of dynamic volume changes at the single-cell level with high time resolution. Collectively, our work highlights how the coupling of FXm with yeast genetics will bring new insights into the complex biology of cell growth.

## INTRODUCTION

Cell volume is a complex trait that is modulated by both genetic and environmental components (Amodeo and Skotheim, 2016; Cook and Tyers, 2007; Lloyd, 2013; Marshall et al., 2012; Mueller, 2015). It has an impact on a host of processes (Pedersen et al., 2001; Zhurinsky et al., 2010), playing important roles in tissue architecture and contributing to the overall size and shape of an organism. At the single-cell level, volume and surface area not only define how cells interact with their environment but also determine their intracellular chemistry and organization. Strikingly, deregulation of cell size has dramatic consequences and is a hallmark of aging and cancer (Li et al., 2015; Pietras, 2011; Yang et al., 2011).

In proliferating cells, volume is linked to cell cycle progression. Specific stages of the cell cycle are associated with differential changes in cell size and morphology, and the dynamics of cell growth are complex across species. For instance, while fission yeast cells stop growing and maintain their shape during mitosis, mammalian cells undergoing division show a transient phase of rounding and volume alteration (Lancaster et al., 2013; Zlotek-Zlotkiewicz et al., 2015). In addition, cell size checkpoints were proposed to be central to the fission yeast cell cycle, allowing for the coordination of growth and division (Fantes, 1977; Fantes and Nurse, 1978; Fantes and Nurse, 1977). These mechanisms reduce cell-to-cell heterogeneity, thereby maintaining size homeostasis. Modulation of cell size is also triggered by environmental changes, and cell cycle exit is often associated with a decrease in cell volume. For example, yeast cells exposed to nitrogen or glucose starvation enter quiescence with a significantly reduced size (Sun and Gresham, 2021). Interestingly, increases in cell volume were observed during long-term experimental evolution in bacteria and proposed to contribute to improved proliferation (Grant et al., 2021; Lenski and Travisano, 1994; Mongold and Lenski, 1996). The volume of dividing cells may therefore result from the necessary balance between growth advantages and evolutionary trade-offs.

The mechanisms underlying size control have been the focus of in-depth investigation. While several pathways have been described (Amodeo and Skotheim, 2016; Cook and Tyers, 2007; Lloyd, 2013; Marshall et al., 2012; Mueller, 2015), whether they represent the key processes that ensure size homeostasis remains unclear. Surprisingly, how cells measure and control their geometric characteristics is still poorly understood, and multiple models that are not mutually exclusive have been proposed: cells may divide 1) when reaching a specific size (sizer), 2) after a defined time following a landmark event (timer) and 3) after having produced a fixed amount of mass, at a rate that depends on birth size (adder). While these possibilities are supported by experimental and theoretical studies (Fantes and Nurse, 1977; Mueller, 2015; Soifer et al., 2016; Sveiczer et al., 1996; Taheri-Araghi et al., 2015), general conclusions are difficult to draw. This may be due in part to the diversity of measurements used to describe cell size, including volume, surface area, length or dry mass. The

question remains whether one or a combination of these characteristics is more relevant for size regulation and whether different cell types rely on the same or distinct parameters. Thus, while the sizes and shapes of individual cell types are considered as hallmarks of cell identity, no unifying principles for size control have emerged.

Experimentally, size regulation has been difficult to investigate, in particular in complex eukaryotes. In mammalian cells, this has been hampered by the challenges of genetic manipulation and the lack of simple methods for accurate measurement of cell volume. Therefore, unicellular eukaryotes such as the budding and fission yeasts remain the models of choice for deciphering the bases of this critical cellular feature, and different concepts have emerged that may provide robust ways of regulating size, including titration mechanisms and dependence on geometric parameters (Amodeo and Skotheim, 2016; Facchetti et al., 2019; Martin and Berthelot-Grosjean, 2009; Moseley et al., 2009). However, how cells monitor their dimensions and how size variation triggers a corrective response is not fully understood.

Due to the cylindrical morphology of fission yeast cells, length at division has been widely used as a proxy for cell size. Despite the ease of measuring cell length, this approach is limited and does not allow for deciphering the complexity of size control. First, cell volume is more critical to cell biology and biochemistry than length. Second, differences in diameter along individual cells (Figs. 1A, B and S1A), which are usually ignored, have a stronger impact on cell volume than length: the size of a rod-shaped cell is linearly dependent on its length but varies with the square and cube of its radius. Finally, length at division restricts the analysis to a small fraction of the population, and morphology mutants or cells grown in conditions that induce alteration of their dimensions cannot be studied using this method. To investigate the control of yeast cell volume, different techniques have been applied. These include volume calculation from geometrical assumptions, 3D reconstruction from 2D imaging data, extrapolation of volume from cell outline detection, and complex approaches using micromechanical devices (Baybay et al., 2020; Bryan et al., 2010; Bryan et al., 2014; Facchetti et al., 2019; Model, 2018; Pan et al., 2014; Zegman et al., 2015). However, these strategies are either low-throughput, difficult to establish or rely on various assumptions and complex image processing. In particular, given the impact of cell diameter on cell volume (Fig. 1A, B and Fig. S1A), accurate evaluation of cell size based on the detection of cell outlines requires these measurements to be highly precise (Baybay et al., 2020; Zegman et al., 2015). Therefore, while these methods represent important steps for addressing size control, a more direct, simple and unbiased technique is necessary.

Recently, a fluorescence exclusion method (FXm) was developed for evaluating the volume of morphologically diverse mammalian cells (Cadart et al., 2018; Cadart et al., 2017). FXm relies on microfluidic devices in which cells are imaged in the presence of a fluorescently-labelled dextran that does not cross the plasma membrane. Thus, using chambers of known height, the local reduction in fluorescence due to the presence of a cell allows for the determination of its volume with high

accuracy (Fig. 1C, (Cadart et al., 2017)). FXm presents a number of advantages over other known and often complex approaches (Bottier et al., 2011; Cadart et al., 2017; Model, 2018; Zlotek-Zlotkiewicz et al., 2015; see also Discussion). It was validated through measurement of artificial substrates of different heights, and data obtained using mammalian cells were highly comparable to those from AFM analyses (Bottier et al., 2011). Furthermore, results from FXm and profilometer measurements for thin PDMS strips were similar (Braïni et al., 2018), highlighting the potential of this method. Importantly, FXm is unaffected by morphological alterations and is compatible with the monitoring of high numbers of cells. However, whether this approach could be used for much smaller cells such as yeast remained unclear, as this would require microdevices with significantly lower internal chambers. For example, HeLa cells are around 20 µm in height with a volume of ~1500 $\mu m^3$ at birth and ~3000 $\mu m^3$ at division (Cadart et al., 2018; Cadart et al., 2019). In contrast, fission yeast cells divide at a length of ~14 µm and a diameter of ~4 µm, with a calculated volume ranging from 120 to 200 $\mu m^3$, depending on growth conditions and width measurements (Navarro and Nurse, 2012; Nurse, 1975).

Here we use the fission yeast as a model and demonstrate that FXm is a groundbreaking tool for measuring the volume of small cells. We engineer specific microdevices for yeast cells, provide an improved pipeline to perform large-scale analyses, and assess the reproducibility and sensitivity of the system. Furthermore, we demonstrate the compatibility of FXm with multi-color imaging for evaluating single-cell volume in specific subpopulations. We finally show that combining FXm with time-lapse experiments will represent a unique strategy for deciphering growth dynamics and size modulation, in particular when taking advantage of yeast genetics. Interestingly, our results suggest that the use of FXm to re-evaluate previous models will be essential for understanding how cell volume is regulated in fission yeast, with implications for the general principles of cell size control in eukaryotes.

## RESULTS

### Microfluidic devices for yeast cell volume measurement

FXm is simple and potentially compatible with cells of any type and shape, making it ideal for investigating size control in genetically amenable models such as yeast. However, to ensure an optimal dynamic range for accurate volume measurements, the height of the microfluidic chamber must be of the same order of magnitude as that of the cells. Indeed, the exclusion of fluorescent molecules in a microsystem several times higher than the cell would only marginally impact the total fluorescence intensity in the region of interest, affecting the reliability of the results. Microdevices employed for mammalian cells are therefore not adapted to fission yeast, which require chambers of ~4-7 µm in height. Interestingly, such reduced dimensions were suggested to be advantageous for the accuracy of FXm (Model, 2020).

This design constraint led us to build specific devices for yeast cells. For this, we determined the optimal pillar density, which has to be high enough to prevent the collapse of the chambers without reducing the throughput of the method. Indeed, cells close to these pillars are excluded from analysis due to the bias introduced in the measurements by the presence of neighboring structures (Cadart et al., 2017). We therefore tested chambers with various inter-pillar distances and found 180 µm (Fig. 1D), coupled with an optimized cell concentration and preparation procedure, to be the most reliable combination for assessing high numbers of cells in a single frame (Fig. 1E, Materials and Methods).

### Measuring single yeast cell volume with FXm

FXm image analysis consists of three steps: image normalization, cell selection and volume calculation. The concepts underlying these different aspects of FXm and the extraction of volume from fluorescence measurements have been thoroughly described (Bottier et al., 2011; Cadart et al., 2017; Zlotek-Zlotkiewicz et al., 2015). However, the use of a low magnification objective (see Materials and Methods), the size of yeast cells and the high number of cells in a frame make it labor-intensive to manually select individual cells using the existing code that was established for mammalian cells. Interestingly, the normalization procedure generates a mask that separates pillars and cells from the background (Cadart et al., 2017). Since the majority of objects extracted at this step corresponds to valid individual cells, we took advantage of this mask and developed a Python script to assist the user in cell selection. Thus, instead of manually delineating each region of interest for analysis (Fig. 2A, top), this tool offers two distinct strategies:

First, a user-guided selection mode can be chosen, in which cells pre-selected by the normalization mask are magnified and individually displayed (Fig. 2A, bottom), allowing the user to rapidly exclude incorrect objects (*e.g.* dust particles, cell aggregates). This makes the analysis of a

large number of cells easier and faster. We validated this method by first assessing the volumes of haploid *vs*. diploid cells and found that diploids were almost twice as large as haploids (1.84 fold, Figs. 2B and S1B). In addition, we analyzed cells with more subtle differences in volume, comparing wild type with the well-described *wee1-50$^{ts}$* (small) and *cdc25-22$^{ts}$* (large) temperature-sensitive cell cycle mutants grown at permissive temperature (Fantes, 1979; Fantes and Nurse, 1978; Nurse, 1975). Our results demonstrated significant differences in volume between these strains (Figs. 2C and S1C). Interestingly, our data for *wee1-50$^{ts}$* were similar to those obtained using a Coulter Multisizer (Table S1, ~5% difference), but the latter reported lower volumes for both wild-type (-19%) and *cdc25-22$^{ts}$* (-23%) cells compared to FXm. This is consistent with a known drawback of the Coulter, which underestimates the size of rod-shaped particles (Bryan et al., 2012; Cavicchi et al., 2015): small *wee1-50$^{ts}$* cells are closer to spherical objects and thus less sensitive to this bias.

Second, an automated selection can be applied. To exclude cell aggregates or small dead cells, a threshold is used based on the interquartile range (IQR) of the population data. This is more appropriate than absolute cut-offs, which need to be adjusted from strain to strain. After testing different approaches, we found that excluding values that are one IQR above or below the third and first quartiles, respectively, was optimal for obtaining results similar to those from the user-guided method (Fig. 2D). Importantly, our code also allows for tuning the outlier threshold and displays the total number of objects as well as the number and percentage of discarded measurements on each side of the spectrum. The user can thus evaluate the quality of the data and apply a manual analysis when necessary.

Finally, our script also integrates the option of separating the selected cells in different groups, making it possible to determine the volumes of distinct subpopulations, for instance based on additional fluorescence markers (see below).

Collectively, our results suggest that FXm can be used for measuring yeast cell volume, and the improvements brought by our analysis code facilitate FXm while providing additional options to the user for more complex studies. Interestingly, while manual selection is the most accurate approach, we show that automated analysis with outlier exclusion allows a rapid assessment of high numbers of cells while remaining sufficiently reliable for screening the volumes of many strains.

## Robustness of FXm for measuring yeast cell volume

The necessity of using microchips of reduced height may represent a challenge for precisely measuring the volume of individual yeast cells. Indeed, in these conditions, the difference between the minimum (pillar) and maximum (no cell) fluorescence intensities (Fig. 1C), as well as the extent of fluorescent molecule displacement in the presence of a cell, are inherently low. This may render the technique more susceptible to noise.

To evaluate whether FXm provides high quality results for yeast, we measured the size of wild-type fission yeast cells, comparing both the median volumes and volume distributions from independent experiments. To this end, we analyzed five replicates from separate devices built from the same 5.53 µm mold. Remarkably, we obtained reproducible data with a median volume for the pooled dataset of 104.8 $\mu m^3$ (standard error, s.e.m.: 1.7 $\mu m^3$; Fig. 3A). This is consistent with previous results established by complex image processing (Baybay et al., 2020), validating FXm for size monitoring in yeast. Comparing our individual datasets, we found that alterations up to ~10% in median volume at the population level can occur between replicates of the same strain. This likely results from biological variations and differences in local or global chamber heights (see Materials and Methods). Thus, changes below this conservative threshold should be interpreted with caution, as they are in the range of the observed experimental variability between replicates. To test if this threshold could be improved by increasing sample size, we used 6 independent measurements and compared all combinations of non-overlapping triplicates ($n$>900 for each pooled dataset). In this context, we found that the maximum difference between two datasets was less than 6.5% (Table S2), suggesting that the threshold for distinguishing strains with different median volumes depends on sample size and number of repeats. Note that when using the geometric model for fission yeast (Fig. 1A) and a constant diameter of 4 µm, an increase of 6.5% in volume at division results from an increase in length at division from 14 to ~14.8 µm. The same alteration in volume with a constant length at division of 14 µm is brought about by an increase in diameter of ~0.1 µm. These changes in length and width are at or below the minimal difference that can be reliably determined by light microscopy in *S. pombe*, thus further highlighting the sensitivity of FXm for yeast cell volume measurement. Finally, we evaluated the reproducibility of the volume distributions observed in our experiments (Table S3) and demonstrated the robustness of FXm for describing the volume profiles of asynchronous populations.

Next, we evaluated potential sources of technical variability associated with FXm. First, inconsistencies in chamber height contribute to differences in volume between replicates (see Materials and Methods). Indeed, we showed that when measuring the respective volumes of two distinguishable wild-type strains within a single chip, the variability threshold can be lowered even when scoring similar numbers of cells (6.6% *vs.* 10%; compare Fig. S2 and Fig. 3A). Importantly, in contrast to the impact of errors in cell width measurements when using conventional approaches (Fig. 1A), FXm data are only linearly affected by differences in chamber dimensions, making this technique less sensitive to experimental variation. Nevertheless, as standard microfabrication procedures make it difficult to generate highly reproducible chamber heights, we set out to assess how changes in the dimensions of different molds may impact volume determination. To this end, we produced microchips of various heights and measured the size of wild-type fission yeast cells by FXm. Surprisingly, the median volumes and volume distributions were comparable (Fig. 3B, Table S3

– median volume of the pooled datasets ~106.8 µm$^3$; s.e.m. for the 5 replicates: 1.9 µm$^3$), showing that data obtained with different devices can be reliably compared. Furthermore, to ascertain measurement noise at the single-cell level beyond chamber height, we determined the volumes of individual cells over a series of 20 successive images acquired every 100 ms (Fig. 3C). Considering that cell size does not significantly change within this 2 s time window, our results show that the variability inherent to FXm is very limited (< 2%), even with such low chambers.

Altogether, these experiments demonstrate that FXm with specifically adapted microfluidic chips is robust and compatible with the analysis of yeast cell volume, producing highly reproducible results.

**Small variations in cell dimensions and population heterogeneity**

Our initial evaluation of FXm experimental variability suggests that changes in median volume ≥ 6.5% between strains or growth conditions can be reliably detected (Fig. 3). To confirm this, we first determined the volume of cells showing a marginal difference in length at division compared to wild type. To this end, we took advantage of a strain whose proliferation relies on a minimal cell cycle control network (MCN). In this background, cell proliferation is solely dependent on a single cyclin/cyclin-dependent kinase (CDK) activity (Coudreuse and Nurse, 2010). Interestingly, while behaving similarly to wild type, MCN cells show a minor increase of ~7% in length at division (Fig. 4A, top). At constant diameter (4 µm), the length values we measured are predicted to contribute to a similar increase in volume according to the geometric model of *S. pombe*. Surprisingly, FXm measurements showed a median volume difference of 17% between these strains (Fig. 4A bottom, Fig. S3A; compare WT and MCN). This suggests that the change in size between wild-type and MCN cells is not solely the result of an increase in cell length (Fig. 4A). Next, building on the results in Fig. 2C and 3A, we compared wild-type cells grown at 32 *vs*. 25 ºC using large sample sizes and 5 independent replicates (Fig. 4B and Fig. S3B). Our analyses established a difference of ~9% in median volume between these conditions. Finally, we investigated whether even smaller alterations in volume at the population level could be detected as cells progressively change size over time. To this end, we used MCN cells, which harbor an alteration in CDK that makes it sensitive to dose-dependent inhibition by non-hydrolysable ATP analogues (Bishop et al., 2000; Coudreuse and Nurse, 2010). This allowed us to synchronize cells at G2/M (Fig. S3C, D) and monitor volume changes throughout the following G2 with high time resolution (Fig. 4C). Even considering the variability at certain time points (-1.3% at T=100 and +0.1% at T=135 compared to T=95 and T=130, respectively), small increases in volume (<5%, Fig. S7A) could be measured. These experiments demonstrate the high sensitivity of FXm in this context.

Another critical parameter in our understanding of cell size homeostasis is the size distribution in the population. This reflects the cell-to-cell heterogeneity in cell cycle progression and the strength of

the size control. Most studies in fission yeast have focused on variability in length at division. However, not only does this exclude the majority of cells, but our results above suggest that evaluating volume distribution may lead to different conclusions. To determine whether FXm allows for monitoring alterations in size profiles, we took advantage of MCN cells in which the target residues of the conserved Wee1/Cdc25 feedback loop on CDK are substituted (T14A Y15F, MCN-AF). Loss of this mitotic switch results in an increase in cell-to-cell variability in length at division (Coudreuse and Nurse, 2010). In our experimental conditions, we found that these cells are shorter than wild type (Fig. 4A). As anticipated, we also observed a broader distribution of cell volume in MCN-AF compared to MCN and wild-type cells (Fig. 4D). Remarkably, the relative changes in median volume *vs.* length at division between MCN-AF, MCN and wild type provide insights into the dimensions that are altered in these strains (Fig. 4A, Table S4): while MCN-AF and MCN appear to differ only in length (same ratios for volume *vs.* length at division), our data suggest that both strains may show an increase in diameter compared to wild type (differing ratios). This was consistent with the measured differences in cell width at division, although they fall below the margin of error (Fig. 4A).

Altogether, these results demonstrate that FXm is easy, sensitive and more robust to experimental errors than previously used methods requiring cell width determination. It enables the monitoring of small alterations in cell volume and changes in size homeostasis in populations of yeast cells. Coupling this approach with traditional cell length measurements is also a promising approach for investigating fission yeast volume regulation, providing novel and more in-depth information on cell size and geometry.

**Measuring the size of cells with altered geometries and morphologies**

The use of length as a proxy for fission yeast size is particularly problematic when studying mutants or conditions where cellular aspect-ratio and shape are altered. Strategies using cell outline detection to extrapolate volume may not be sufficiently reliable in this situation, given the influence of minor changes in diameter on cell volume.

In this context, we determined the volumes of various strains showing defects in morphology and shape by FXm. First, we assessed strains lacking Rga2, Rga4 or Rga6, which are members of the RhoGAP family. These factors are involved in polarized growth, and their loss impacts cell geometry (Das et al., 2007; Revilla-Guarinos et al., 2016; Soto et al., 2010; Villar-Tajadura et al., 2008). When ranking these strains according to their lengths at division, we found that Δ*rga2* cells are the longest, followed by Δ*rga6* and Δ*rga4* (Fig. 5A). Strikingly, FXm, which is independent of cell geometry, led to the opposite conclusion, with Δ*rga4* and Δ*rga2* cells having the largest and smallest volumes, respectively (Fig. 5B, Fig. S4A).

Next, we assessed the size of cells for which length can be difficult to measure or inherently inaccurate due to morphological alterations. To this end, we used bent cells *(Δknk1, Δtea1)* as well as cells with significant shape defects and irregular diameters (Δ*mal3*) (Beinhauer et al., 1997; Mata and Nurse, 1997; Scheffler et al., 2014) (Fig. 5C). As anticipated, while cell length at division could not be determined without excluding a significant fraction of the cells, FXm allowed us to establish the profiles of cell volume in these populations and compare them with wild-type cells (Fig. 5D, Fig. S4B). This again highlights the power of this method for studying size control mechanisms independently of cell morphology. Interestingly, in cells with abnormal shapes, both the median volume and size distribution may change (Fig. 5A-D, Fig. S4), potentially reflecting alteration of their cell cycle organization and associated growth patterns. This opens the door to investigating how cell shape may delineate the complex interplay between growth and division at the single-cell level.

Finally, we evaluated FXm data for significantly smaller cells that have stopped dividing. Upon glucose exhaustion, fission yeast cells exit the cell cycle and enter quiescence, which is associated with a dramatic reduction in size. Given the shape of these arrested cells (Fig. 5E), determining their length and width to extrapolate their volume is unreliable. In contrast, FXm established high-quality profiles of cell volume for these populations (Fig. 5F, Fig. S5). This will allow for investigating the impact of cell size on cell physiology and aging in this critical cellular state.

Collectively, this set of experiments demonstrates the versatility of FXm, which provides an unprecedented ability to measure the size of any strain, irrespective of cell morphology and physiological status. Our results also suggest that previous conclusions on size control in fission yeast may need to be re-evaluated using FXm.

**Measuring the volume of subpopulations**

The experiments presented so far have focused on the determination of cell volume in entire populations. However, extracting the size of cells in specific subpopulations is critical for understanding how different processes may interact with the mechanisms that underlie cell size control and how cell growth and proliferation are coupled. Thus, combining FXm with intracellular fluorescent markers would represent a powerful method to take advantage of yeast genetics and explore the complexity of size regulation in different conditions and throughout the cell cycle. Similarly, this could allow for discriminating between distinct strains expressing specific markers in a complex population, opening the door to exploring non-cell autonomous processes that may affect volume regulation.

As a proof-of-concept, we determined cell volume at mitosis, using the non-histone chromatin-associated protein Nhp6 coupled to mCherry. First, we validated that nuclear Nhp6::mCherry did not induce any significant signal in the FITC channel under FXm conditions (Fig. S6A). This also showed

that the slightly reduced volume of these cells compared to wild type (Fig. 6A, Fig. S6B) results from an alteration of Nhp6 function due to the tag rather than a bias from mCherry fluorescence. Using our improved FXm code, we segmented the population of binucleated cells (~11% of the total number of cells) and determined their median volume (~126.5 µm$^3$, compared to ~93.5 µm$^3$ for mononucleated cells, Fig. 6B). The partial overlap between mono- and binucleated cells is consistent with the interruption of growth during mitosis: cell size does not change during nuclear division, and growth only resumes in G1. Note that the volume of binucleated cells measured in our assay is consistent with previous calculations of cell volume at division (Nurse, 1975) but differs from those presented in a more recent study (Navarro and Nurse, 2012). Altogether, our experiments validate the possibility of combining FXm with additional markers in yeast for more complex investigations of cell size control and dynamics.

**Dynamic changes in fission yeast cell volume at the population and single-cell levels**

Next, we tested FXm for assessing dynamic changes in yeast cell size. First, we ascertained whether coupling time course experiments with FXm allows for following induced alterations in cell volume over time using asynchronous populations. A wide range of growth conditions (*e.g.* heat stress (Vjestica et al., 2013), osmotic stress (Millar et al., 1995), change in nutrient availability (Fantes and Nurse, 1977; Petersen, 2009)) as well as experimental modulation of specific cellular pathways can trigger cell size changes. Understanding the dynamics of such changes may be key to determining the implication of these processes in cell size homeostasis. To evaluate FXm in this context, we took advantage of the analog-sensitivity of MCN cells. Indeed, reducing CDK activity in fission yeast using this method leads to an increase in cell size (Chen et al., 2016; Coudreuse and Nurse, 2010). We therefore measured cell volume in asynchronous MCN cells at 40 minute intervals (~1/4 of the cell cycle) after treatment with 0.05 µM 3-MBPP1 (Fig. 7). Our data show that MCN cells progressively increase their volume, up to 1.7-fold after one doubling time. Strikingly, comparison of the volume *vs.* length at division ratios throughout the experiment (Table S4) suggests complex dynamics in the respective modulations of length and diameter upon CDK inhibition. This demonstrates that FXm 1) can be used to follow short-term alterations in median cell size and size distribution in asynchronous yeast populations and 2) provides new perspectives for our understanding of how the geometrical dimensions of cells contribute to their volume.

We then asked if FXm could be applied to analyze individual yeast cells in time-lapse experiments. To this end, the injection inlets in our chips were enlarged (from 2.5 to 4 mm), acting as nutritional reservoirs to maintain stable growth conditions. As fission yeast cells are non-adherent, this assay also required pre-coating of the chip coverslips with lectin. In this setup, we observed a linear increase in volume during each cell cycle and a plateau in size around the time of cell division,

corresponding to the well-described growth arrest at mitosis (Mitchison, 1957; Mitchison and Nurse, 1985) (Fig. 8A). However, cells divided at smaller sizes in succeeding cell cycles, suggesting that the built-in reservoirs are insufficient to ensure a favorable growth environment throughout our assay. We therefore applied a constant flow of fresh medium containing FITC-Dextran (~3-5 µL.min$^{-1}$) for the entire duration of the experiments. Using this method, we did not detect any consistent reduction in cell volume at division after each cycle (Fig. 8B). Furthermore, the growth rate (see Materials and Methods) was significantly higher than without medium renewal (Fig. 8).

These data demonstrate that FXm is a unique tool for monitoring the volume dynamics of small cells with a high time resolution and for detecting changes in growth rate at the single-cell level. This will allow for investigating the immediate responses of cells to environmental perturbations and the behaviors of separate yeast cell lineages. In addition, this will make it possible to relate volume at birth, growth rate and volume at division for a given cell. Coupled with additional markers, this technique thus offers an unprecedented entry into the investigation of cell size control and its interplay with other complex cellular processes.

## DISCUSSION

Regulation of cell volume is critical for eukaryotic organisms, but the mechanisms underlying this process are still unclear. Yeast models have played a pioneering role in deciphering this complex trait and remain at the forefront of this very active research field. However, the difficulty of accurately measuring cell volume in these small unicellular organisms has been an obstacle for our understanding of size control and homeostasis. Here we show that the fluorescence exclusion method (FXm) is ideal for evaluating the volume of yeast cells in diverse contexts. It provides high quality data on the volume profiles of yeast populations irrespective of cell morphology and physiological state, allows for single-cell analysis of volume changes with high time resolution and is compatible with the use of additional fluorescent markers. Our experiments also demonstrate that FXm gives researchers unique access to in-depth analyses of yeast cell volume dynamics and their coupling with cell cycle progression, integrating the size of cells at all stages of their division cycle. Furthermore, combining FXm with time-lapse imaging represents an unprecedented tool for exploring the changes in growth rate and cellular geometry that occur not only during proliferation or upon major transitions such as quiescence entry and exit, but also when cells respond to acute challenges.

In addition to the versatility and power of this method, FXm is cost-effective and easy to implement. All steps of the microfabrication process, from generating the molds to producing the chips, can be performed using standard microfabrication techniques that are now widespread and available within many research teams or in the constantly increasing number of microfabrication facilities. FXm does not require complex microscopy setups, allows for the rapid measurement of a high number of cells and is less biased by measurement errors compared to strategies that rely on cell width. Furthermore, it is based on single-plane imaging, limiting bleaching and phototoxicity, and is not affected by the position of each cell along the z-axis, a particular advantage when using non-adherent cells. Finally, the treatment of FXm images is simple and does not require advanced segmentation processes or high computing power. At this stage, the main drawback of FXm is in the measurement of the volumes of individual cells within colonies and dense populations: this requires manual segmentation of each cell, and the direct proximity to a high number of other cells impacts the results. Thus, given the limited disadvantages of FXm compared to its ease of implementation, robustness and accuracy, we believe that this technique will become a new standard for investigating cell size control in yeast, with implications for our knowledge of size regulation in complex eukaryotes.

Interestingly, our work led to a number of observations that may question existing models of cell size regulation. First, research on *S. pombe* size control and its interplay with cell cycle progression has mostly been based on the assumption that the diameter of proliferating haploid fission yeast cells is 1) constant from one cell to another and 2) homogenous along their growing axis. Our results clearly indicate that these assumptions can lead to incorrect conclusions when comparing strains, as

shown using various mutants (Figs. 4, 5). In this context, FXm has the advantage of being a direct method for volume measurement that does not rely on any pre-conceived idea of cell geometry. Coupling FXm with cell length measurements also offers an additional level of understanding of cell size dynamics. For example, our data suggest that when cells are arrested in their division cycle through CDK inhibition, the geometric changes that occur over time are surprisingly complex, with length and volume alterations showing different kinetics (Table S4, MCN + 3-MBPP1). Similarly, we find that simplifying the architecture of cell cycle control or growing cells in distinct environments has unanticipated impacts on cell geometry, affecting both cell length and diameter (Table S4).

Focusing on subpopulations, as is the case when using cell length at division as a proxy for cell size, may also hamper our comprehension of important processes linking cell growth, morphology and proliferation. For instance, the apparent changes in size distribution that we observed in morphology mutants suggest that the interplay between growth rate and cell cycle phases may be altered in these cells. This may shed light on potentially novel inputs and mechanisms that modulate cell size dynamics. In this context, the different cell geometries of *rga* mutants, as indicated by our comparisons of volume *vs*. cell length at division ratios (Table S4), may represent a promising strategy for uncovering the key parameters used by cells to "monitor" their size.

Our work demonstrates that previous models that describe the way cell size is regulated in fission yeast need to be revisited using FXm. Together with the wealth of knowledge on size control in this organism, this approach will provide new insights into the processes that underlie the biology of cell growth. Interestingly, the investigation of cellular processes has been enriched by the use of natural yeast isolates. In fission yeast, these strains are known to be less homogenous in morphology and overall size (Jeffares et al., 2015). FXm may therefore make it possible to fully exploit this unique resource and take advantage of advanced population genetics strategies to decipher the regulation of cell size. While we use fission yeast as a proof-of-concept model, our results also show that FXm can be applied to any type of cell over a broad range of sizes. Our studies therefore establish the versatility and power of FXm for investigating cell volume homeostasis and its regulation in small cells and model organisms, contributing to our general understanding of the modulation of cellular dimensions and scaling in eukaryotes.

## MATERIALS AND METHODS

### Fission yeast strains and methods

Standard methods and media were used (Hayles and Nurse, 1992; Moreno et al., 1991). All the strains used in this study are detailed in Table S5. The deletions of *rga2*, *rga4*, *rga6*, *mal3*, *knk1* and *tea1* have already been described (Soto et al., 2010; Villar-Tajadura et al., 2008; Beinhauer et al., 1997; Mata and Nurse, 1997; Revilla-Guarinos et al., 2016; Scheffler et al., 2014). All experiments were carried out in non-supplemented minimal medium (EMM) at 32 ºC, except otherwise noted. To inhibit CDK activity in analog-sensitive MCN strains, the 3-MBPP1 inhibitor (A602960, Toronto Research Chemicals, Inc.) was dissolved in DMSO at stock concentrations of 10 or 0.4 mM and added to liquid cultures at a final concentration of 1 or 0.05 µM. The percentage of binucleated cells (Fig. S3D) was determined from heat fixed samples on microscope slides (70 ºC for 5 min) stained with a 11:1 solution of Blankophor (1 mg/mL): DAPI (1 µg/mL).

### Measurement of cell volume using a Coulter Multisizer

Cells were grown in EMM at 25 ºC and resuspended in dedicated cuvettes containing Isoton (Beckman Coulter, USA). Cell volume was measured using a Coulter Multisizer 4 (Beckman Coulter, USA) with a 30 µm aperture tube.

### Microfabrication of FXm chips

PDMS microfluidic chips for FXm were prepared following standard microfabrication protocols (McDonald and Whitesides, 2002). In brief, master molds were made by spin-coating SU-8 2005 resin (MicroChem Corp., USA) on silicon wafers using a spincoater (Laurell Technologies, USA) according to manufacturer's instructions. Microstructures were then generated using high-resolution chrome masks (JD phototools, UK) and 365nm UV exposure (UV KUB 3, Kloe, France) followed by PGMEA (Sigma-Aldrich) development. For each mold, the height of the structures was determined as the average of three measurements perpendicular to the long axis of the design (Fig. 1D) using a Veeco Wyko NT9100 optical profilometer (Veeco Instruments Inc., USA). Molds showing significant variability between the three height measurements were discarded. Nevertheless, local variations in chip dimensions may occur during the microfabrication process. When using a single averaged chamber height, biases may therefore be introduced in the evaluation of cell size depending on the position of the cell in the chip. Thus, when even higher accuracy is needed, further reduction of the experimental error can be achieved by using regional chamber heights. For this, the chip can be divided into sub-areas, identifying each area by introducing markers in the mask used for microfabrication and measuring the height of each area using a profilometer. Volume determination can then be made with more specific parameters depending on the position of the cell within the chamber.

To produce chips for FXm, a 10:1 mixture of PDMS (Sylgard 184, Dow Corning, USA) was cast on the SU-8 master mold and allowed to cure at 70 °C for 2 hours. Inlets were then made using 2.5 or 4 mm biopsy punches, and chips were bonded to microscopy-grade coverslips by plasma activation (Harrick Plasma, USA). As the pillars are used not only to support the chip ceiling but also for the normalization and volume calculation (Cadart et al., 2017), particular attention must be paid to the integrity of these structures and their proper bonding to the coverslip. In addition, for accurate measurements, we recommend using freshly fabricated chips.

**Preparation of fission yeast cells for FXm**

To perform FXm experiments, exponentially growing fission yeast cells were sampled at an optical density between 0.25 and 0.45 at 595 nm ($OD_{595}$). To limit the formation of cell aggregates, a mild sonication cycle of 5 s at 10% amplitude (Branson 450 Digital Sonifier, Emerson Electric Co.) was applied. This treatment had no effect on the results we obtained by FXm (data not shown). In order to maximize the number of cells that can be measured on a single FXm image in our chip design, cells were concentrated to ~$5.5x10^7$ cells/mL in their own conditioned minimal medium (note that to prevent bias in our volume measurements, we did not use rich medium, which is autofluorescent). FITC-Dextran was then added to the sample (FD10S, Sigma Aldrich) at a final concentration of 1 mg/mL, and cells were loaded into the chip shortly before image acquisition. For evaluating the volume of quiescent cells, cells were grown in EMM at 32 °C and sampled 24 hours after they reached $OD_{595}$ = 0.4.

**Microscopy**

All microscopy experiments were carried out using an inverted Zeiss Axio Observer (Carl Zeiss Microscopy LLC) equipped with a Lumencor Spectra X illumination system and an Orca Flash 4.0V2 sCMOS camera (Hamamatsu Photonics). Acquisition was performed using the VisiView software (Visitron Systems GmbH). A Plan-Apochromat 63X/1.4 NA immersion lens and a Plan-Apochromat 20X/0.8 NA Ph2 lens (Carl Zeiss Microscopy LLC) were used for cell length measurements and FXm, respectively. FXm requires the capture of all the fluorescence from the area of the chamber under observation (Cadart et al., 2017). This is most easily achieved using low magnification lenses with low numerical apertures. Higher magnification objectives with low NA may be compatible with FXm and the chamber height used in our experiments. However, as a reference, we tested FXm with a 63X/1.4 NA lens (Carl Zeiss Microscopy LLC) and found that it led to a slight overestimation of cell volume (data not shown), as is expected when not all fluorescence light from the chamber is acquired. Thus, comparing the data from a 20X low NA with those obtained using a given high-magnification lens is a pre-requisite for performing robust FXm analysis with such an objective. For routine volume measurements, the acquisition parameters were 100 ms exposure at 20% illumination power, and 30

to 40 images were taken across the entire chamber to limit potential bias due to local changes in chamber height. For the time-lapse experiments in Fig 8, 100 ms exposure at 10% illumination power was used.

**Image analysis**

Cell length and width at division were determined from Blankophor images (1 mg/mL Blankophor solution, A108741, Ambeed Inc.) using FIJI (National Institutes of Health) and the Pointpicker plug-in. For the blankophor images in Fig. 2, 4, 5, 6 and 7, brightness and contrast were adjusted for display purposes. For routine volume measurements, images were first normalized using a custom Matlab software (Cadart et al., 2017). This code can be obtained from M. Piel upon request (matthieu.piel@curie.fr). Cell selection and volume calculation were subsequently performed using the normalization mask with a new, specifically-developed Python interface (see Results, script available at https://github.com/SyntheCell/select-pombe-fxm/). For all figures except Figs. 2D, 4C and 8, cell selection was done using the manual mode. For Figs. 2D and 4C, automated cell identification was used. Our Python code is not adapted to tracking the volume of individual cells in long time-lapse experiments (Fig. 8), as slight cell movements make it difficult to reliably follow single cells over time when using the normalization mask pre-selection. For these assays, we therefore used the original Matlab software (Cadart et al., 2017). Note that except for the time-lapses in Fig. 8, we systematically excluded cells that were undergoing cytokinesis but that had not fully separated into two individual daughter cells; this population is similarly excluded in studies using cell length at division.

**FXm time-lapse and analysis using fission yeast**

As fission yeast cells are non-adherent, FXm time-lapses required coverslips to be coated in order to prevent cells from moving inside the chambers, which would hamper data acquisition and analysis. To this end, 10 µL of 1mg/mL filtered lectin was spread in a rectangle of ~10x5 mm at the center of the coverslips and allowed to dry at 37 ºC. The coverslips were then washed once with filtered ultra-pure water and dried at 37 ºC. For experiments without medium flow (Fig. 8A), Ø 4 mm inlets were made in the PDMS chips using the appropriate biopsy punch. 5 µL of cells prepared as described above were loaded in one inlet, and both inlets were then filled with 45 µL EMM containing the FITC-Dextran dye. Cells were then allowed to flow into the chambers prior to imaging. For time-lapse experiments using medium flow (Fig. 8B), two successive layers of lectin were applied as above and inlets of Ø 0.75 mm were fabricated. Cells were then loaded by depositing a drop of cells prepared as above over one of the inlets, and a mild vacuum was applied at the other inlet using the tip of a 10 mL pipet connected to a vacuum pump. The loaded chip was then connected to a flow control system (pressure generator and flow controller, Elvesys, France), and a flow of medium (~3-5 µL/min) containing the FITC-Dextran dye was used throughout the experiment. For the time-lapse

experiments, the two daughter cells after a division were manually delineated during the analysis and only one of them was followed for further investigation (Fig. 8). To validate this manual segmentation, we measured the same 10 pairs of sister cells at birth 5 consecutive times. This led to an average coefficient of variation for all 20 cells of 0.019 +/- 0.011 (standard deviation, s.d.), corresponding to a precision of 1.1%. Similarly, the total volume of each pair of sister cells was measured 5 consecutive times, and we compared the average value of these 5 measurements with the sum of the average volumes of each sister cells determined as above. The average of the relative difference between total volume and sum of sister cell volumes for all 10 pairs was 1.3 +/- 1.0% (s.d.). The growth rate of each cell was determined by calculating the slopes of the traces during each cycle. This was obtained by linear regression considering the volume at birth (when an invagination is detected) as the first time point and excluding the mitotic plateau: entry into mitosis was assigned to the last point prior to a strong reduction of growth (when two consecutive points on the graph decrease the slope).

**Statistical analyses**

All statistical analyses were performed in Python using the SciPy module (Fig. 4D, 6A, Table S3).

## ACKNOWLEDGMENTS

We thank Pei-Yun Jenny Wu and Snezhana Oliferenko for critically reading the manuscript. We thank Pascal Hersen and Giacomo Gropplero for the measurements of our chamber heights. We are grateful to Damien Laporte for performing the Coulter Counter analyses. We thank Paul Nurse, Snezhana Oliferenko, Pilar Perez and Phong Tran for sharing strains and reagents.

## COMPETING INTERESTS

No competing interests declared.

## FUNDING

This work was supported by a grant to DC from the Agence Nationale de la Recherche (ANR, project eVOLve, ANR-18-CE13-0009; funding for AJ and DGR) and the Région Bretagne (ARED Pombevol, funding for DGR). JCR was supported by a fellowship from the Ministère de l'Enseignement Supérieur et de la Recherche. LV was supported by a grant to DC from the Région Nouvelle Aquitaine (CHESS 2022). VRB was supported by an ERC Starting Grant to DC (SyntheCycle, Grant Agreement no. 310849).

## REFERENCES


**Amodeo, A. A. and Skotheim, J. M.** (2016). Cell-Size Control. *Cold Spring Harb Perspect Biol* **8**, a019083.

**Baybay, E. K., Esposito, E. and Hauf, S.** (2020). Pomegranate: 2D segmentation and 3D reconstruction for fission yeast and other radially symmetric cells. *Scientific reports* **10**, 16580–15.

**Beinhauer, J. D., Hagan, I. M., Hegemann, J. H. and Fleig, U.** (1997). Mal3, the fission yeast homologue of the human APC-interacting protein EB-1 is required for microtubule integrity and the maintenance of cell form. *The Journal of cell biology* **139**, 717–728.

**Bishop, A. C., Ubersax, J. A., Petsch, D. T., Matheos, D. P., Gray, N. S., Blethrow, J., Shimizu, E., Tsien, J. Z., Schultz, P. G., Rose, M. D., et al.** (2000). A chemical switch for inhibitor-sensitive alleles of any protein kinase. *Nature* **407**, 395–401.

**Bottier, C., Gabella, C., Vianay, B., Buscemi, L., Sbalzarini, I. F., Meister, J.-J. and Verkhovsky, A. B.** (2011). Dynamic measurement of the height and volume of migrating cells by a novel fluorescence microscopy technique. *Lab Chip* **11**, 3855–3863.

**Braïni, C., Mottolese, A., Ferrante, I., Monnier, S. and Villard, C.** (2018). High-resolution Volume Imaging of Neurons by the Use of Fluorescence eXclusion Method and Dedicated Microfluidic Devices. *J Vis Exp* e56923.

**Bryan, A. K., Engler, A., Gulati, A. and Manalis, S. R.** (2012). Continuous and long-term volume measurements with a commercial Coulter counter. *PloS one* **7**, e29866.

**Bryan, A. K., Goranov, A., Amon, A. and Manalis, S. R.** (2010). Measurement of mass, density, and volume during the cell cycle of yeast. *Proc. Natl. Acad. Sci. U.S.A.* **107**, 999–1004.

**Bryan, A. K., Hecht, V. C., Shen, W., Payer, K., Grover, W. H. and Manalis, S. R.** (2014). Measuring single cell mass, volume, and density with dual suspended microchannel resonators. *Lab Chip* **14**, 569–576.

**Cadart, C., Monnier, S., Grilli, J., Sáez, P. J., Srivastava, N., Attia, R., Terriac, E., Baum, B., Cosentino-Lagomarsino, M. and Piel, M.** (2018). Size control in mammalian cells involves modulation of both growth rate and cell cycle duration. *Nat Commun* **9**, 3275–15.

**Cadart, C., Venkova, L., Recho, P., Lagomarsino, M. C. and Piel, M.** (2019). The physics of cell-size regulation across timescales. *Nat. Phys.* **15**, 993–1004.

**Cadart, C., Zlotek-Zlotkiewicz, E., Venkova, L., Thouvenin, O., Racine, V., Le Berre, M., Monnier, S. and Piel, M.** (2017). Fluorescence eXclusion Measurement of volume in live cells. *Methods Cell Biol.* **139**, 103–120.

**Cavicchi, R. E., Carrier, M. J., Cohen, J. B., Boger, S., Montgomery, C. B., Hu, Z. and Ripple, D. C.** (2015). Particle shape effects on subvisible particle sizing measurements. *J Pharm Sci* **104**, 971–987.

**Chen, T., Gómez-Escoda, B., Munoz-Garcia, J., Babic, J., Griscom, L., Wu, P.-Y. J. and Coudreuse, D.** (2016). A drug-compatible and temperature-controlled microfluidic device for live-cell imaging. *Open Biol* **6**, 160156.

**Cook, M. and Tyers, M.** (2007). Size control goes global. *Curr. Opin. Biotechnol.* **18**, 341–350.

**Coudreuse, D. and Nurse, P.** (2010). Driving the cell cycle with a minimal CDK control network. *Nature* **468**, 1074–1079.

**Das, M., Wiley, D. J., Medina, S., Vincent, H. A., Larrea, M., Oriolo, A. and Verde, F.** (2007). Regulation of cell diameter, For3p localization, and cell symmetry by fission yeast Rho-GAP Rga4p. *Molecular biology of the cell* **18**, 2090–2101.

**Facchetti, G., Knapp, B., Flor-Parra, I., Chang, F. and Howard, M.** (2019). Reprogramming Cdr2-Dependent Geometry-Based Cell Size Control in Fission Yeast. *Current biology : CB* **29**, 350–358.e4.

**Fantes, P.** (1979). Epistatic gene interactions in the control of division in fission yeast. *Nature* **279**, 428–430.

**Fantes, P. A.** (1977). Control of cell size and cycle time in Schizosaccharomyces pombe. *J. Cell. Sci.* **24**, 51–67.

**Fantes, P. A. and Nurse, P.** (1978). Control of the timing of cell division in fission yeast. Cell size mutants reveal a second control pathway. *Experimental cell research* **115**, 317–329.

**Fantes, P. and Nurse, P.** (1977). Control of cell size at division in fission yeast by a growth-modulated size control over nuclear division. *Experimental cell research* **107**, 377–386.

**Grant, N. A., Abdel Magid, A., Franklin, J., Dufour, Y. and Lenski, R. E.** (2021). Changes in Cell Size and Shape during 50,000 Generations of Experimental Evolution with Escherichia coli. *Journal of bacteriology* **203**.

**Hayles, J. and Nurse, P.** (1992). Genetics of the fission yeast Schizosaccharomyces pombe. *Annu. Rev. Genet.* **26**, 373–402.

**Jeffares, D. C., Rallis, C., Rieux, A., Speed, D., Převorovský, M., Mourier, T., Marsellach, F. X., Iqbal, Z., Lau, W., Cheng, T. M. K., et al.** (2015). The genomic and phenotypic diversity of Schizosaccharomyces pombe. *Nature genetics* **47**, 235–241.

**Lancaster, O. M., Le Berre, M., Dimitracopoulos, A., Bonazzi, D., Zlotek-Zlotkiewicz, E., Picone, R., Duke, T., Piel, M. and Baum, B.** (2013). Mitotic rounding alters cell geometry to ensure efficient bipolar spindle formation. *Dev. Cell* **25**, 270–283.

**Lenski, R. E. and Travisano, M.** (1994). Dynamics of adaptation and diversification: a 10,000-generation experiment with bacterial populations. *Proc. Natl. Acad. Sci. U.S.A.* **91**, 6808–6814.

**Li, Q., Rycaj, K., Chen, X. and Tang, D. G.** (2015). Cancer stem cells and cell size: A causal link? *Semin. Cancer Biol.* **35**, 191–199.

**Lloyd, A. C.** (2013). The regulation of cell size. *Cell* **154**, 1194–1205.

**Marshall, W. F., Young, K. D., Swaffer, M., Wood, E., Nurse, P., Kimura, A., Frankel, J., Wallingford, J., Walbot, V., Qu, X., et al.** (2012). What determines cell size? *BMC Biol.* **10**, 101.

**Martin, S. G. and Berthelot-Grosjean, M.** (2009). Polar gradients of the DYRK-family kinase Pom1 couple cell length with the cell cycle. *Nature* **459**, 852–856.

**Mata, J. and Nurse, P.** (1997). tea1 and the microtubular cytoskeleton are important for generating global spatial order within the fission yeast cell. *Cell* **89**, 939–949.

**McDonald, J. C. and Whitesides, G. M.** (2002). Poly(dimethylsiloxane) as a material for fabricating microfluidic devices. *Acc. Chem. Res.* **35**, 491–499.

**Millar, J. B., Buck, V. and Wilkinson, M. G.** (1995). Pyp1 and Pyp2 PTPases dephosphorylate an osmosensing MAP kinase controlling cell size at division in fission yeast. *Genes & development* **9**, 2117–2130.

**Mitchison, J. M.** (1957). The growth of single cells. I. Schizosaccharomyces pombe. *Experimental cell research* **13**, 244–262.

**Mitchison, J. M. and Nurse, P.** (1985). Growth in cell length in the fission yeast Schizosaccharomyces pombe. *J. Cell. Sci.* **75**, 357–376.

**Model, M.** (2020). Comparison of cell volume measurements by fluorescence and absorption exclusion microscopy. *J Microsc* **280**, 12–18.

**Model, M. A.** (2018). Methods for cell volume measurement. *Cytometry A* **93**, 281–296.

**Mongold, J. A. and Lenski, R. E.** (1996). Experimental rejection of a nonadaptive explanation for increased cell size in Escherichia coli. *Journal of bacteriology* **178**, 5333–5334.

**Moreno, S., Klar, A. and Nurse, P.** (1991). Molecular genetic analysis of fission yeast Schizosaccharomyces pombe. *Meth. Enzymol.* **194**, 795–823.

**Moseley, J. B., Mayeux, A., Paoletti, A. and Nurse, P.** (2009). A spatial gradient coordinates cell size and mitotic entry in fission yeast. *Nature* **459**, 857–860.

**Mueller, R. L.** (2015). Genome Biology and the Evolution of Cell-Size Diversity. *Cold Spring Harb Perspect Biol* **7**, a019125.

**Navarro, F. J. and Nurse, P.** (2012). A systematic screen reveals new elements acting at the G2/M cell cycle control. *Genome Biol.* **13**, R36.

**Nurse, P.** (1975). Genetic control of cell size at cell division in yeast. *Nature* **256**, 547–551.

**Pan, K. Z., Saunders, T. E., Flor-Parra, I., Howard, M. and Chang, F.** (2014). Cortical regulation of cell size by a sizer cdr2p. *Elife* **3**, e02040.

**Pedersen, S. F., Hoffmann, E. K. and Mills, J. W.** (2001). The cytoskeleton and cell volume regulation. *Comp. Biochem. Physiol., Part A Mol. Integr. Physiol.* **130**, 385–399.

**Petersen, J.** (2009). TOR signalling regulates mitotic commitment through stress-activated MAPK and Polo kinase in response to nutrient stress. *Biochem. Soc. Trans.* **37**, 273–277.

**Pietras, A.** (2011). Cancer stem cells in tumor heterogeneity. *Adv. Cancer Res.* **112**, 255–281.

**Revilla-Guarinos, M. T., Martín-García, R., Villar-Tajadura, M. A., Estravís, M., Coll, P. M. and Pérez, P.** (2016). Rga6 is a Fission Yeast Rho GAP Involved in Cdc42 Regulation of Polarized Growth. *Molecular biology of the cell*.

**Scheffler, K., Recouvreux, P., Paoletti, A. and Tran, P. T.** (2014). Oscillatory AAA+ ATPase Knk1 constitutes a novel morphogenetic pathway in fission yeast. *Proc. Natl. Acad. Sci. U.S.A.* **111**, 17899–17904.

**Soifer, I., Robert, L. and Amir, A.** (2016). Single-Cell Analysis of Growth in Budding Yeast and Bacteria Reveals a Common Size Regulation Strategy. *Current biology : CB* **26**, 356–361.

**Soto, T., Villar-Tajadura, M. A., Madrid, M., Vicente, J., Gacto, M., Pérez, P. and Cansado, J.** (2010). Rga4 modulates the activity of the fission yeast cell integrity MAPK pathway by acting as a Rho2 GTPase-activating protein. *The Journal of biological chemistry* **285**, 11516–11525.

**Sun, S. and Gresham, D.** (2021). Cellular quiescence in budding yeast. *Yeast* **38**, 12–29.

**Sveiczer, A., Novak, B. and Mitchison, J. M.** (1996). The size control of fission yeast revisited. *J. Cell. Sci.* **109 ( Pt 12)**, 2947–2957.

**Taheri-Araghi, S., Bradde, S., Sauls, J. T., Hill, N. S., Levin, P. A., Paulsson, J., Vergassola, M. and Jun, S.** (2015). Cell-size control and homeostasis in bacteria. *Current biology : CB* **25**, 385–391.

**Villar-Tajadura, M. A., Coll, P. M., Madrid, M., Cansado, J., Santos, B. and Pérez, P.** (2008). Rga2 is a Rho2 GAP that regulates morphogenesis and cell integrity in S. pombe. *Mol. Microbiol.* **70**, 867–881.

**Vjestica, A., Zhang, D., Liu, J. and Oliferenko, S.** (2013). Hsp70-Hsp40 chaperone complex functions in controlling polarized growth by repressing Hsf1-driven heat stress-associated transcription. *PLOS Genetics* **9**, e1003886.

**Yang, J., Dungrawala, H., Hua, H., Manukyan, A., Abraham, L., Lane, W., Mead, H., Wright, J. and Schneider, B. L.** (2011). Cell size and growth rate are major determinants of replicative lifespan. *Cell cycle* **10**, 144–155.

**Zegman, Y., Bonazzi, D. and Minc, N.** (2015). Measurement and manipulation of cell size parameters in fission yeast. *Methods Cell Biol.* **125**, 423–436.

**Zhurinsky, J., Leonhard, K., Watt, S., Marguerat, S., Bähler, J. and Nurse, P.** (2010). A coordinated global control over cellular transcription. *Current biology : CB* **20**, 2010–2015.

**Zlotek-Zlotkiewicz, E., Monnier, S., Cappello, G., Le Berre, M. and Piel, M.** (2015). Optical volume and mass measurements show that mammalian cells swell during mitosis. *The Journal of cell biology* **211**, 765–774.

## FIGURE LEGENDS

**Figure 1. Cell volume and microfluidic chips for FXm. A.** The geometric model of a fission yeast cell is based on a cylinder with half spheres at both ends. Differences in radius thus have a stronger impact on volume than those in cell length. **B.** Distribution of the coefficients of variation (CV) of cell volume at division for 25 cells, determined using the geometric model. For each cell, length at division and width at 5 different positions were measured (Fig. S1A). Cell volume was then calculated using each width measurement and the CV was determined for each cell. **C.** Schematic of the principles of FXm. Top: cells are injected in a FXm chip (see *D*) in the presence of FITC-Dextran. Pillars are integrated for ceiling support and image normalization. Single-plane images (see *E*) are acquired for analysis. Bottom: after normalization, cell volume is determined from the loss of fluorescence (grey area, the internal height of the chip must be measured). Although this schematic represents the fluorescence along a scan line for ease of visualization, FXm relies on the assessment of fluorescence intensity over the entire area in which the cell of interest is located. **D.** Schematic of the chambers used for fission yeast. Left: design and dimensions (not to scale). Right: pillars are 60 µm in diameter and separated by 180 µm. **E.** Image of fission yeast cells in an FXm experiment (before image normalization).

**Figure 2. Measuring yeast cell volume by FXm. A.** Top: representative image showing the selection of individual cells using the original FXm code. Each valid cell must be identified from the FITC image (Fig. 1E; the area shown has been magnified for display purposes) and the regions of interest (hexagons) manually drawn for quantification. Bottom: representative image showing the new FXm pipeline, which takes advantage of the normalization mask for cell selection. All objects are automatically identified and displayed individually at higher magnification. Cell aggregates (bottom left), recently-divided cells (bottom right) or artifacts can be excluded by the user (red-barred). **B.** Top: comparison of volume distributions in populations of wild-type haploid and diploid fission yeast cells by FXm. Cells were grown in EMM6S at 32 °C. Pooled datasets ($n \geq 1073$) for three independent experiments ($n \geq 207$ for each replicate, Fig. S1B). Values outside of the plot range ($n^*$) were excluded: $n^* \leq 1$ for each replicate. Bottom: blankophor images, cell length at division (LAD) is indicated (averages with standard deviations - s.d. - for pooled datasets of three independent experiments, $n \geq 100$ for each replicate). Scale bars = 10 µm. In EMM6S, wild-type cells have a volume similar to that in EMM (compare with Figs. 3-7) but a reduced LAD (compare with Fig. 4A, 5A, 6 and 7), suggesting a difference in cell width between these conditions. **C.** Top: wild type (WT), *wee1-50*$^{ts}$ and *cdc25-22*$^{ts}$ temperature-sensitive strains were grown at the permissive temperature of 25 °C and their volumes measured by FXm. Pooled datasets ($n \geq 1144$) of three independent experiments ($n \geq 337$ for each replicate, Fig. S1C). $n^* \leq 6$ for each replicate. Bottom: blankophor images with LAD (averages with s.d. for pooled datasets of three independent experiments, $n \geq 100$ for each replicate).

Scale bars = 10 µm. At 25 °C, WT cells have a reduced volume and LAD compared to 32 °C (compare with Figs. 3-7). **D.** Comparison of FXm results using manual (black) *vs.* automated (grey, 1 IQR filter) cell selection. Data for manual selection are from Fig. 2C. For automated selection, 1) the same images as for the manual method were used, pooling data from all replicates, and 2) a filter was applied that excludes entries that are 1 IQR above and below Q3 and Q1 ($n^{**}$), respectively (unfiltered selected objects: $n \geq 1390$, excluded objects $n^{**} \leq 200$). The overlap between the two approaches for both correctly assigned cells and outliers is between 87 and 92%. *B-D*: graphs are histograms with box and whiskers plots, indicating the min, Q1, median (white dot), Q3 and max, with outliers determined by 1.5 IQR (interquartile range). Median volumes with median absolute deviations (m.a.d) are shown.

**Figure 3. Robustness of FXm for measuring yeast cell volume. A.** Measurements of wild-type fission yeast in five independent experiments (grey) and the total pooled dataset (black). Chamber height: 5.53 µm; $n \geq 316$ for each replicate, $n=2266$ for the total dataset; $n^{*} \leq 1$ for each replicate. **B.** Measurements of wild-type cells from a single culture using five distinct devices of the indicated heights (grey) and the total pooled dataset (black). $n \geq 225$ for each replicate, $n=1777$ for the total dataset; $n^{*}=0$ for each replicate. *A, B*: Graphs are as in Fig. 2. **C.** 20 consecutive FXm images were acquired (100 ms exposure per image over a total time of 2 s) and the volumes of 81 individual cells were followed throughout the experiment (left panel). For display purposes, 20 representative cells are shown. The generation time of wild-type cells in these conditions is ~140 min. The coefficients of variation (CV) in volume were determined for each cell (right panel). The average CV for all 81 cells is 0.0071 +/- 0.0028, corresponding to a precision in cell volume measurement of 0.71%.

**Figure 4. FXm detects subtle changes in cell volume and size distribution. A.** Top: blankophor images with LAD and width at division (WAD) (averages with s.d. for pooled datasets of three independent experiments, $n \geq 100$ and $n \geq 60$ per replicate for LAD and WAD, respectively). While the changes in WAD are consistent with our conclusions based on FXm and LAD (see below), they should be interpreted with caution as these differences are below the limit of reliable measurement. Scale bars = 10 µm. Bottom: volume measurement of WT, MCN and MCN-AF cells by FXm. Pooled datasets ($n \geq 913$) of three independent experiments ($n \geq 172$ for each replicate – Fig. S3A). $n^{*} \leq 1$ for each replicate. Graphs are as in Fig. 2. **B.** Comparison of the median volumes (in $\mu m^3$) for 5 independent replicates of WT at 25 and 32 °C. Full datasets are in Fig. S3B. Difference in median cell volume: 8.8%. **C**. MCN cells grown in EMM6S at 32 °C were G2-arrested using 1 µM 3-MBPP1 for 160 min and allowed to synchronously re-enter the cell cycle by washing off the inhibitor (Coudreuse and Nurse, 2010) (Fig. S3C). 50 min after release, cells were injected in a FXm chip and images were

acquired at 5 min intervals throughout the next G2, after the first round of mitosis and cell division (60 min, Fig. S3D). Top: median volumes at the indicated time points (black line – automated cell selection) with IQR (grey area). The higher volume for MCN cells compared to other Figures results from the initial G2 block, during which cells grow without dividing. Cell cycle phases are indicated. G2 growth rate: 0.59 $\mu m^3.min^{-1}$ (linear regression from 60 to 110 min, before the mitotic plateau). As anticipated, no growth was observed during mitosis. From 125 to 140 min, the automated selection does not separate newly divided cells (17.4%, 25.9% and 25.5% of the selected objects at 130, 135 and 140 min, respectively, are pairs of cells; the remainder of the cells have not undergone cytokinesis at these time points). This results in an apparent increased growth rate after mitosis, although additional time points would be required for a robust conclusion. The delay in cell cycle progression compared to Fig. S3D is likely due to the growth conditions in the chips in the absence of medium flow (see Fig. 8A). For each time point, $214 \leq n \leq 278$ (unfiltered automatically selected objects). Outliers were removed using the 1 IQR filter (see Fig. 2D $28 \leq n^{**} \leq 49$, representing a maximum of 18% of the number of selected objects). Bottom: representative images of cells in FXm chips at 85 min (G2), 120 min (M) and 135 min (pairs of cells represent a significant subset of the population at this time, see above). **D.** Volume distribution for the indicated strains as a percentage of the median volume. Data are as in *A*. $n^* \leq 10$. The two-sample Kolmogorov-Smirnov test was used for comparing population distributions. *: $p$-value < 0.05; n.s.: non-significant ($p$-value > 0.05).

**Figure 5. Measuring the volume of yeast cells with altered morphologies. A, C.** Blankophor images. *A*: LAD and WAD are indicated (averages with s.d. for pooled datasets of three independent experiments, $n \geq 100$ and $n \geq 60$ for each replicate for LAD and WAD, respectively). As for Fig. 4A, such small differences in WAD should be interpreted with caution. *C*: LAD is indicated (averages with s.d. for pooled datasets of three independent experiments, $n \geq 100$ for each replicate). n.d.: not determined. Scale bars = 10 µm. **B.** Volume measurement by FXm of the strains in *A*. Pooled datasets ($n \geq 832$) of three independent experiments ($n \geq 268$ for each replicate – Fig. S4A). $n^* \leq 1$ for each replicate. **D.** Volume measurement by FXm of the strains in *C*. Pooled datasets ($n \geq 940$) of three independent experiments ($n \geq 230$ for each replicate – Fig. S4B) are shown. $n^* = 0$ for each replicate. Data for WT are from Fig. 2B (haploids). **E.** Blankophor images of WT cells in exponential growth and quiescence. For quiescent cells, samples were taken 24 h after the culture reached $OD_{595}$ 0.4. For proliferating cells, LAD is shown (average with s.d. for pooled dataset of three independent experiments, $n \geq 100$ for each replicate). n.d.: not determined. Scale bars = 10 µm. **F.** Volume measurement by FXm of the cells in *E*. Pooled datasets ($n \geq 965$) of three independent experiments ($n \geq 238$ for each replicate – Fig. S5). $n^* = 0$ for each replicate. *C, D*: Experiments were carried out in EMM6S due to the presence of auxotrophies in some of the strains (Table S5). *B, D, F*: Graphs are as in Fig. 2.

**Figure 6. FXm is compatible with the use of fluorescent markers to study subpopulations. A.** Top: volume measurement of WT and cells expressing *nhp6::mCherry* by FXm. Pooled datasets ($n \geq 1568$) of three independent experiments ($n \geq 499$ for each replicate – Fig. S6B). $n^* = 0$ for each replicate. Median volume values with m.a.d. are shown. The difference in median volume is above the 6.5% threshold (Mood's test: $p$-value$<10^{-8}$). The two-sample Kolmogorov-Smirnov test was used for comparing population distributions on normalized data: $p$-value=0.96, indicating that the distributions are not different. Bottom: blankophor images with cell length at division of the strains above (averages with s.d. for pooled datasets of three independent experiments, $n \geq 110$ for each replicate). Scale bars = 10 µm. **B.** Volume comparison between mono- (grey) and bi-nucleated (black) cells in the population of *nhp6::mCherry* cells as in *A*. The percentages and median volumes with m.a.d. for the mono- ($n=1619$) and binucleated ($n=196$) subpopulations are indicated. Binucleated cells include both septated (dashed line) and non-septated cells. *A*, *B*: Graphs are as in Fig. 2.

**Figure 7. Dynamic changes in cell volume at the population level.** Left: FXm measurement of MCN cells after treatment with 0.05 µM 3-MBPP1. Untreated WT cells were used as a control. For MCN, samples were collected every 40 min after addition of inhibitor ($n \geq 265$ at each time point, $n=528$ for WT). $n^* \leq 2$ for each dataset. Graphs are as in Fig. 2. Right: blankophor images with average cell length at division and s.d.. $n \geq 100$ for WT and MCN (0, 120 and 160 min). For the 40 and 80 min time points, the initial delay in mitosis due to inhibitor treatment leads to a reduction in the number of dividing cells, making it difficult to obtain similar numbers for the calculation of cell length at division ($n=45$ and 22, respectively). Septation indices: WT: 11.5%, MCN 0 min: 20.4%, MCN 40 min: 1%, MCN 80 min: 2%, MCN 120 min: 15.5%, MCN 160 min: 26.9%; $n \geq 400$ for each time point. Scale bars = 10 µm.

**Figure 8. Real-time monitoring of single-cell volume by FXm. A.** FXm time-lapse experiment using WT in EMM at 32 °C without medium flow. **B.** FXm time-lapse experiment using WT in EMM at 32 °C with a constant flow of medium (3-5 µL.min$^{-1}$) containing FITC-Dextran. *A*, *B*: individual traces represent the volume dynamics of single-cell lineages (at each division, only one of the two daughter cells is further monitored). This approach allows for measuring differences in single-cell volume that are close to the experimental noise determined in Fig. 3C (see Fig. S7B). Volumes were measured every 10 and 5 min for *A* and *B*, respectively. For display purposes, the traces are aligned to the first division (Materials and Methods). Average growth rates with s.d. are shown for each cycle. The growth rate in *B* is consistent with that obtained from the bulk analysis of a synchronized population (Fig. 4C).

**FIGURE 1**

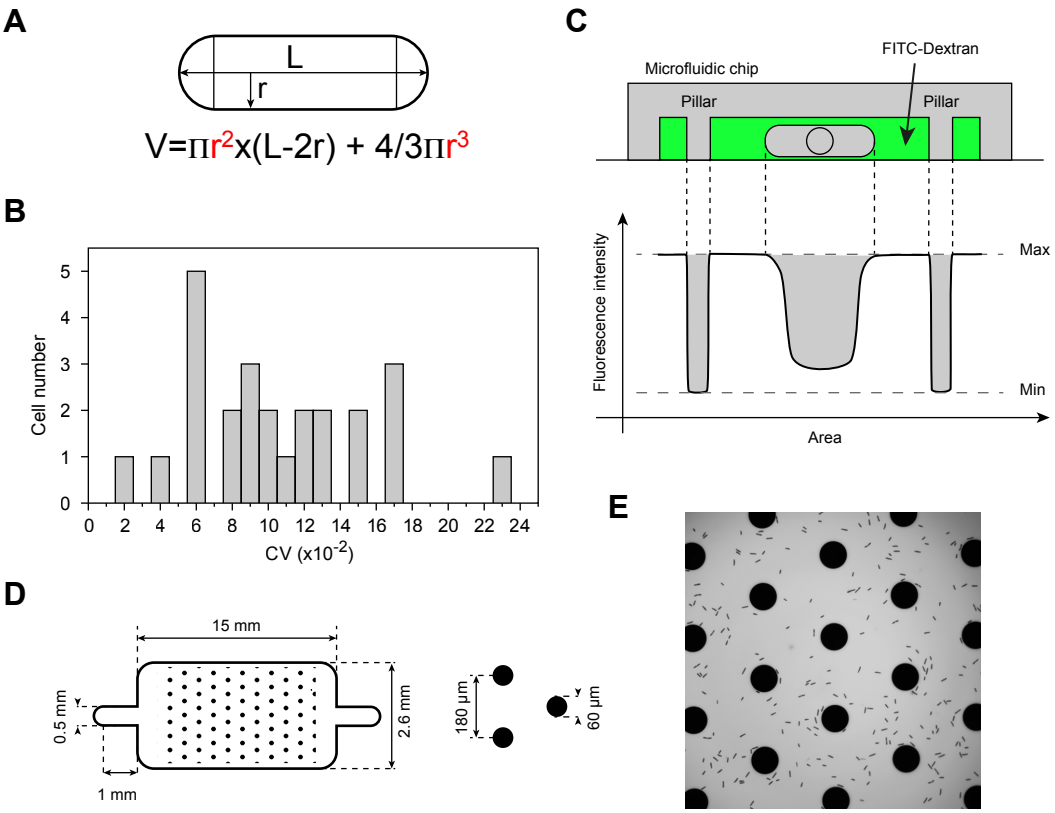
A
L
r
V=Πr2x(L-2r) + 4/3Πr3
B
Cell number
CV (x10-2)
C
Microfluidic chip
FITC-Dextran
Pillar
Pillar
Fluorescence intensity
Max
Min
Area
D
15 mm
0.5 mm
2.6 mm
1 mm
180 µm
60 µm
E

**FIGURE 2**

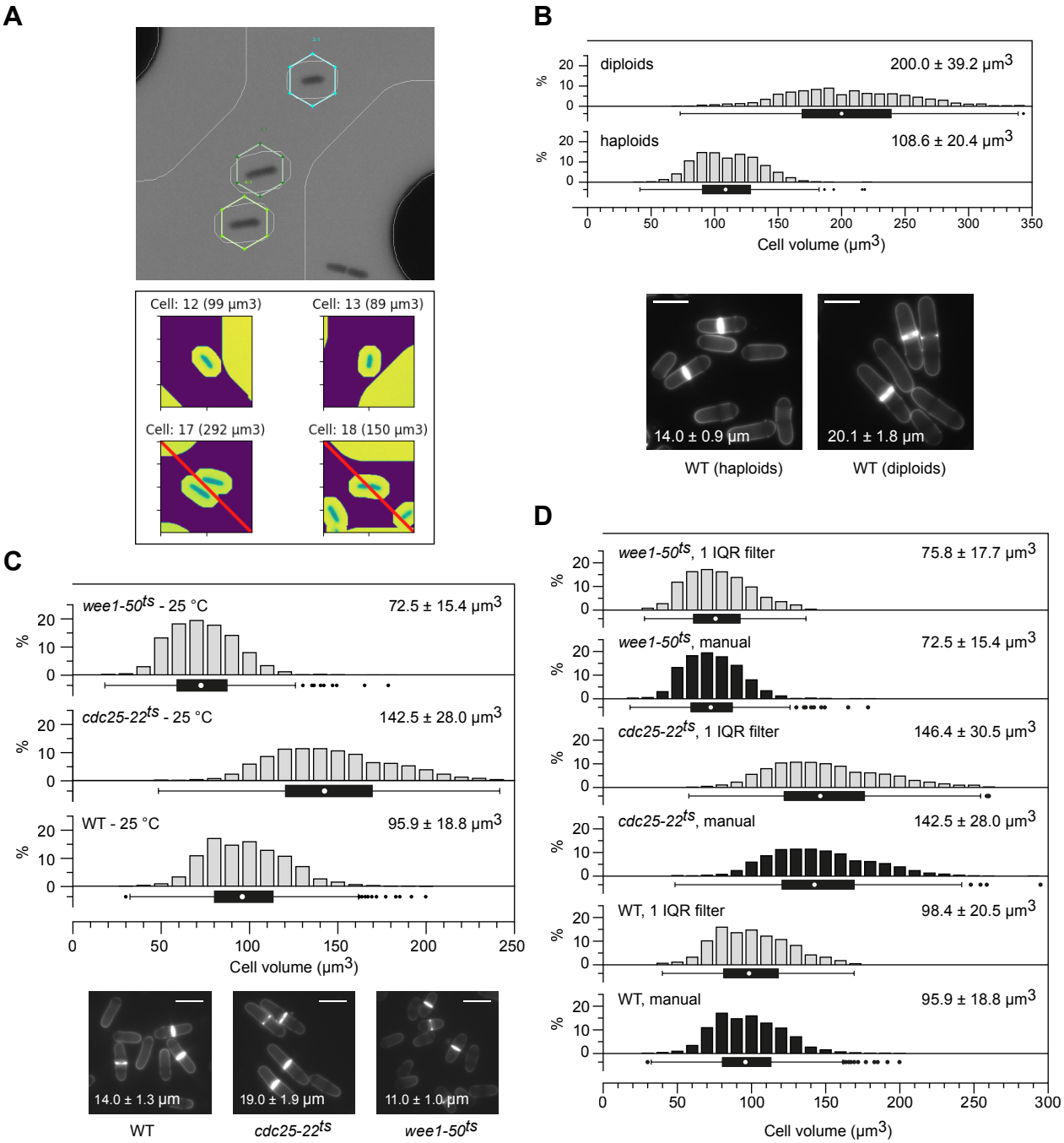
A
Cell: 12 (99 µm3)
Cell: 13 (89 µm3)
Cell: 17 (292 µm3)
Cell: 18 (150 µm3)
B
diploids
200.0 ± 39.2 µm3
haploids
108.6 ± 20.4 µm3
%
Cell volume (µm3)
14.0 ± 0.9 µm
20.1 ± 1.8 µm
WT (haploids)
WT (diploids)
C
wee1-50ts - 25 °C
72.5 ± 15.4 µm3
cdc25-22ts - 25 °C
142.5 ± 28.0 µm3
WT - 25 °C
95.9 ± 18.8 µm3
Cell volume (µm3)
14.0 ± 1.3 µm
19.0 ± 1.9 µm
11.0 ± 1.0 µm
WT
cdc25-22ts
wee1-50ts
D
wee1-50ts, 1 IQR filter
75.8 ± 17.7 µm3
wee1-50ts, manual
72.5 ± 15.4 µm3
cdc25-22ts, 1 IQR filter
146.4 ± 30.5 µm3
cdc25-22ts, manual
142.5 ± 28.0 µm3
WT, 1 IQR filter
98.4 ± 20.5 µm3
WT, manual
95.9 ± 18.8 µm3
Cell volume (µm3)

**FIGURE 3**

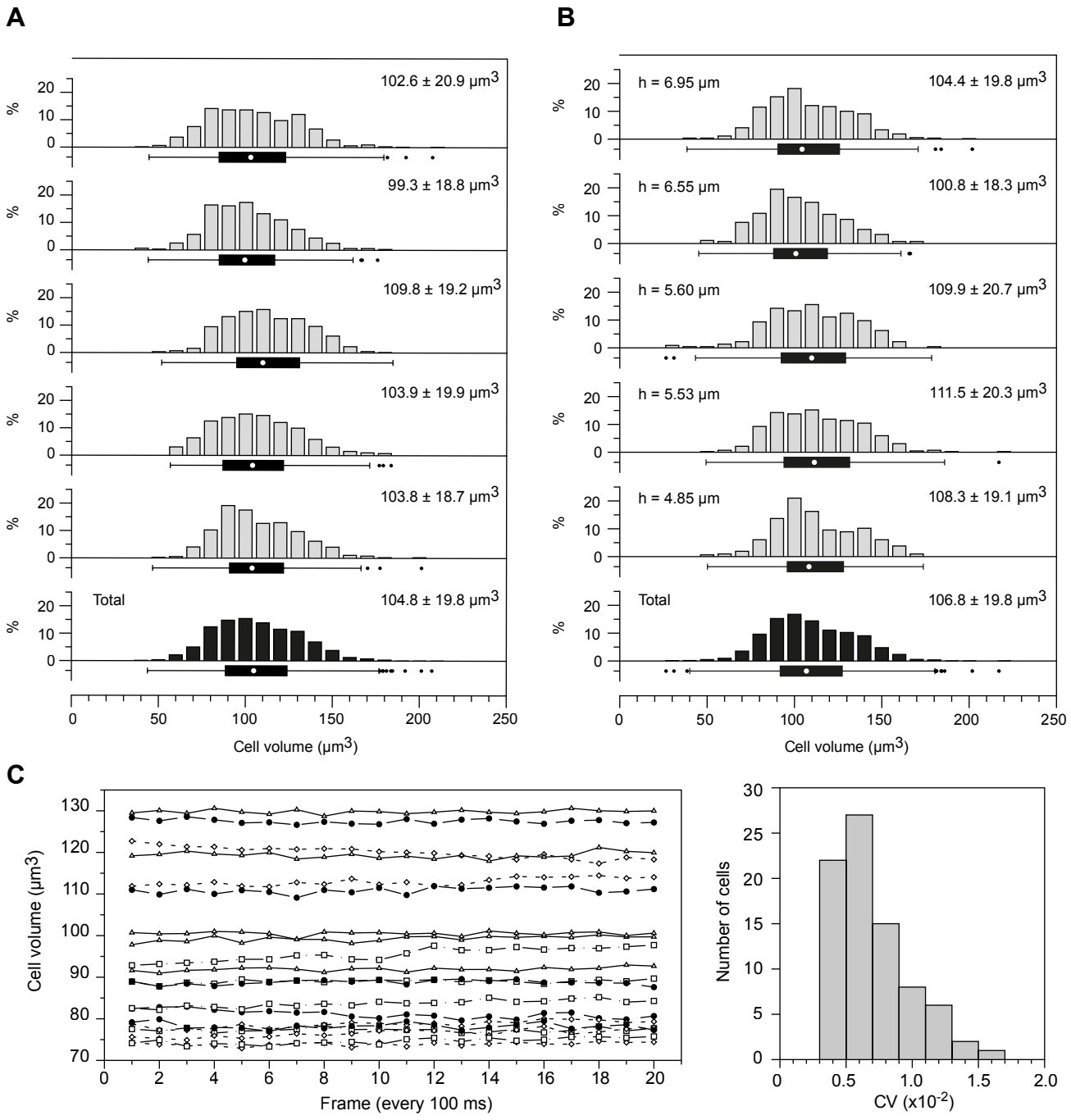
A
B
C
102.6 ± 20.9 µm3
99.3 ± 18.8 µm3
109.8 ± 19.2 µm3
103.9 ± 19.9 µm3
103.8 ± 18.7 µm3
Total
104.8 ± 19.8 µm3
h = 6.95 µm
104.4 ± 19.8 µm3
h = 6.55 µm
100.8 ± 18.3 µm3
h = 5.60 µm
109.9 ± 20.7 µm3
h = 5.53 µm
111.5 ± 20.3 µm3
h = 4.85 µm
108.3 ± 19.1 µm3
Total
106.8 ± 19.8 µm3
%
Cell volume (µm3)
Cell volume (µm3)
Frame (every 100 ms)
Number of cells
CV (x10-2)

# FIGURE 4

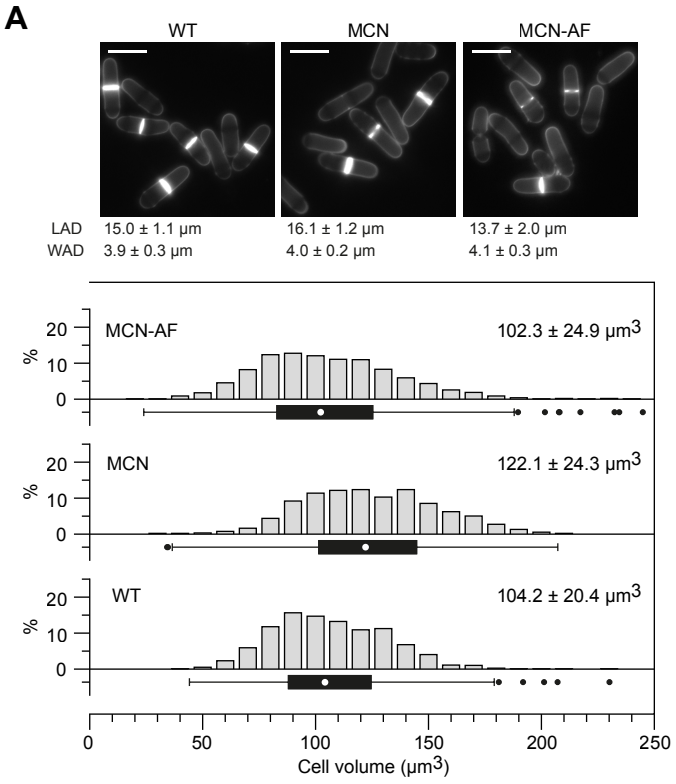


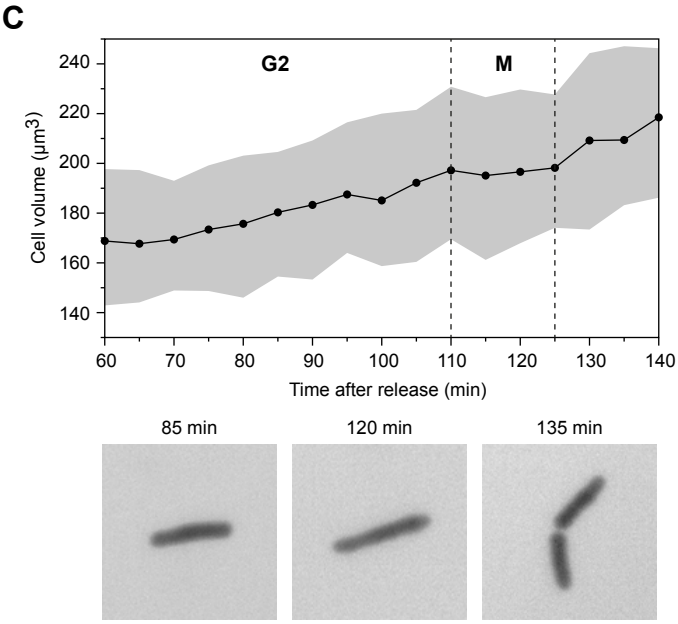


B

| 25 °C | 32 °C |
|---|---|
| 99.1 ± 17.6 | 109.8 ± 19.2 |
| 97.8 ± 17.5 | 103.9 ± 19.9 |
| 94.2 ± 16.1 | 103.8 ± 18.7 |
| 93.6 ± 19.3 | 102.6 ± 20.9 |
| 93.3 ± 16.7 | 99.3 ± 18.8 |
| **Full datasets: 96.3 ± 17.7** | **104.8 ± 19.8** |

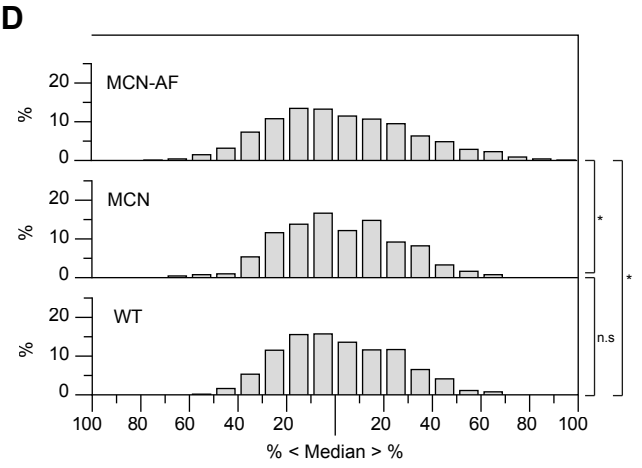

**FIGURE 5**

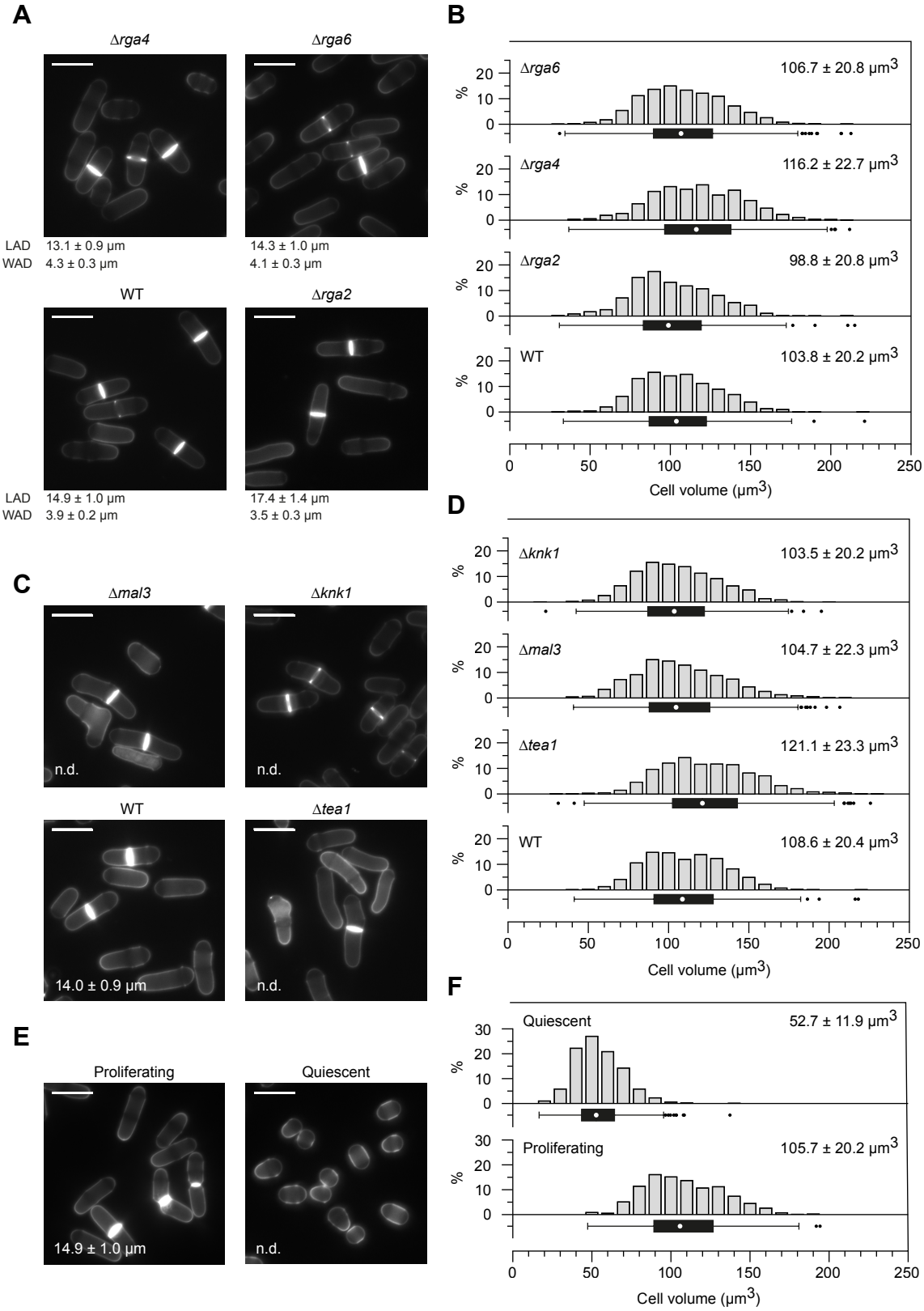
A
Δrga4
Δrga6
LAD 13.1 ± 0.9 μm
WAD 4.3 ± 0.3 μm
14.3 ± 1.0 μm
4.1 ± 0.3 μm
WT
Δrga2
LAD 14.9 ± 1.0 μm
WAD 3.9 ± 0.2 μm
17.4 ± 1.4 μm
3.5 ± 0.3 μm
B
Δrga6 106.7 ± 20.8 μm3
Δrga4 116.2 ± 22.7 μm3
Δrga2 98.8 ± 20.8 μm3
WT 103.8 ± 20.2 μm3
%
Cell volume (μm3)
C
Δmal3
Δknk1
n.d.
n.d.
WT
Δtea1
14.0 ± 0.9 μm
n.d.
D
Δknk1 103.5 ± 20.2 μm3
Δmal3 104.7 ± 22.3 μm3
Δtea1 121.1 ± 23.3 μm3
WT 108.6 ± 20.4 μm3
Cell volume (μm3)
E
Proliferating
Quiescent
14.9 ± 1.0 μm
n.d.
F
Quiescent 52.7 ± 11.9 μm3
Proliferating 105.7 ± 20.2 μm3
Cell volume (μm3)

**FIGURE 6**

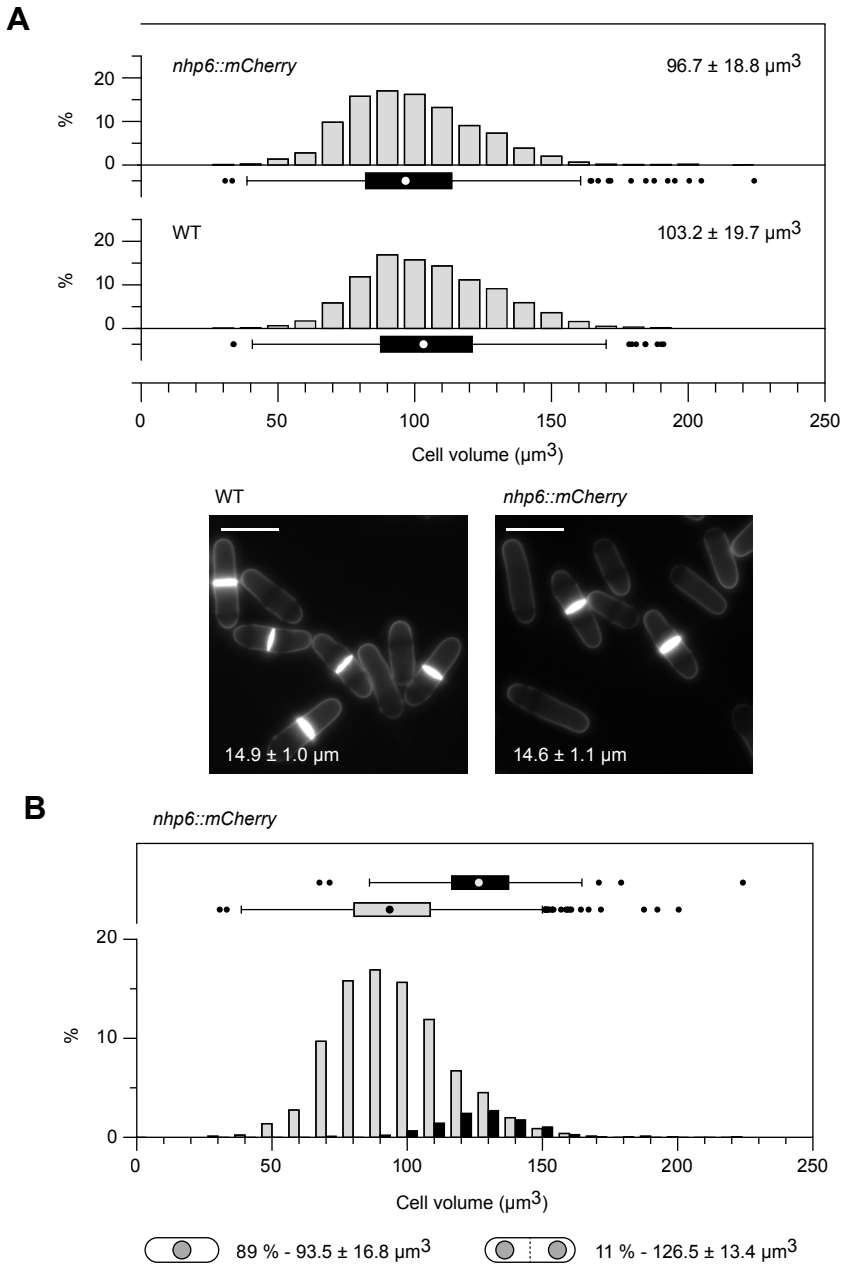
A
nhp6::mCherry
96.7 ± 18.8 µm3
WT
103.2 ± 19.7 µm3
%
20
10
0
0
50
100
150
200
250
Cell volume (µm3)
WT
nhp6::mCherry
14.9 ± 1.0 µm
14.6 ± 1.1 µm
B
nhp6::mCherry
89 % - 93.5 ± 16.8 µm3
11 % - 126.5 ± 13.4 µm3

**FIGURE 7**

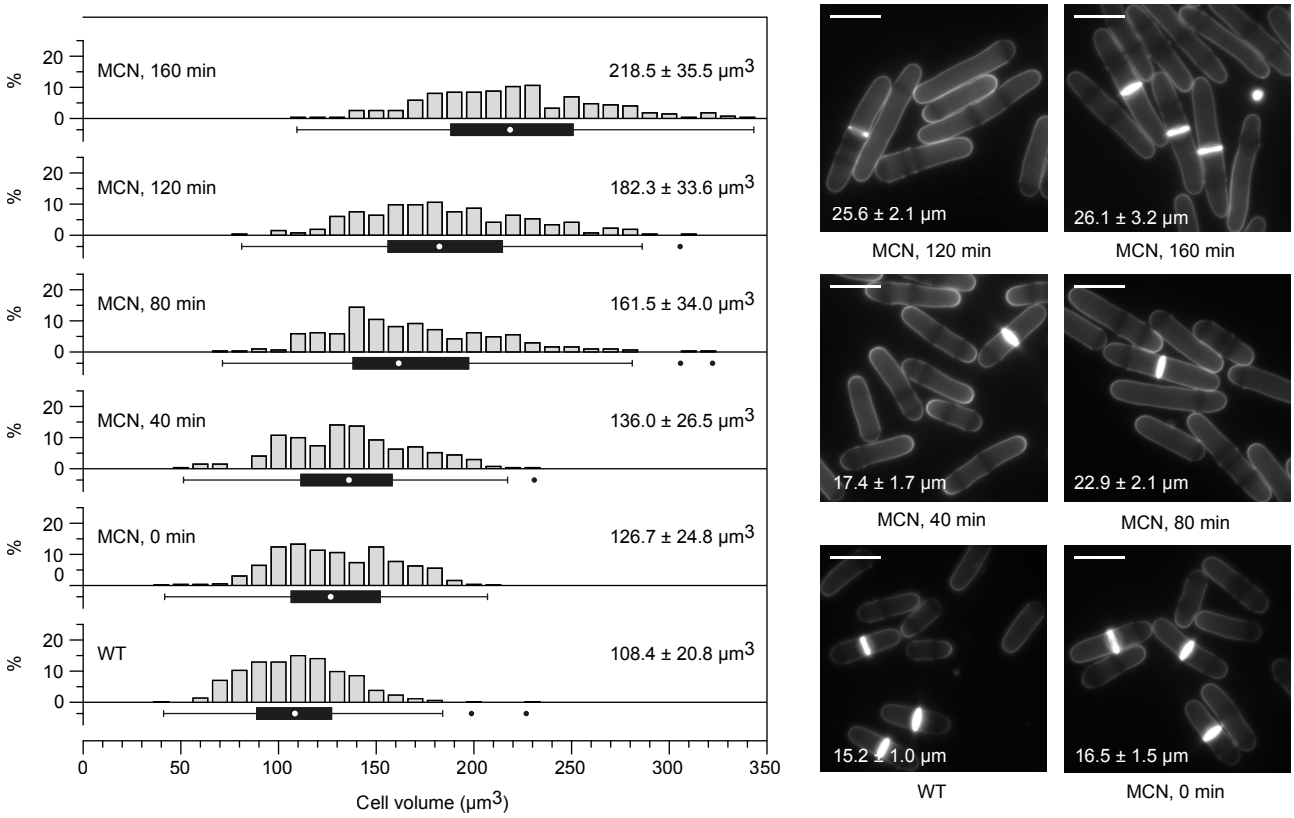
MCN, 160 min
218.5 ± 35.5 µm3
MCN, 120 min
182.3 ± 33.6 µm3
MCN, 80 min
161.5 ± 34.0 µm3
MCN, 40 min
136.0 ± 26.5 µm3
MCN, 0 min
126.7 ± 24.8 µm3
WT
108.4 ± 20.8 µm3
%
0
10
20
0
50
100
150
200
250
300
350
Cell volume (µm3)
25.6 ± 2.1 µm
MCN, 120 min
26.1 ± 3.2 µm
MCN, 160 min
17.4 ± 1.7 µm
MCN, 40 min
22.9 ± 2.1 µm
MCN, 80 min
15.2 ± 1.0 µm
WT
16.5 ± 1.5 µm
MCN, 0 min

**FIGURE 8**

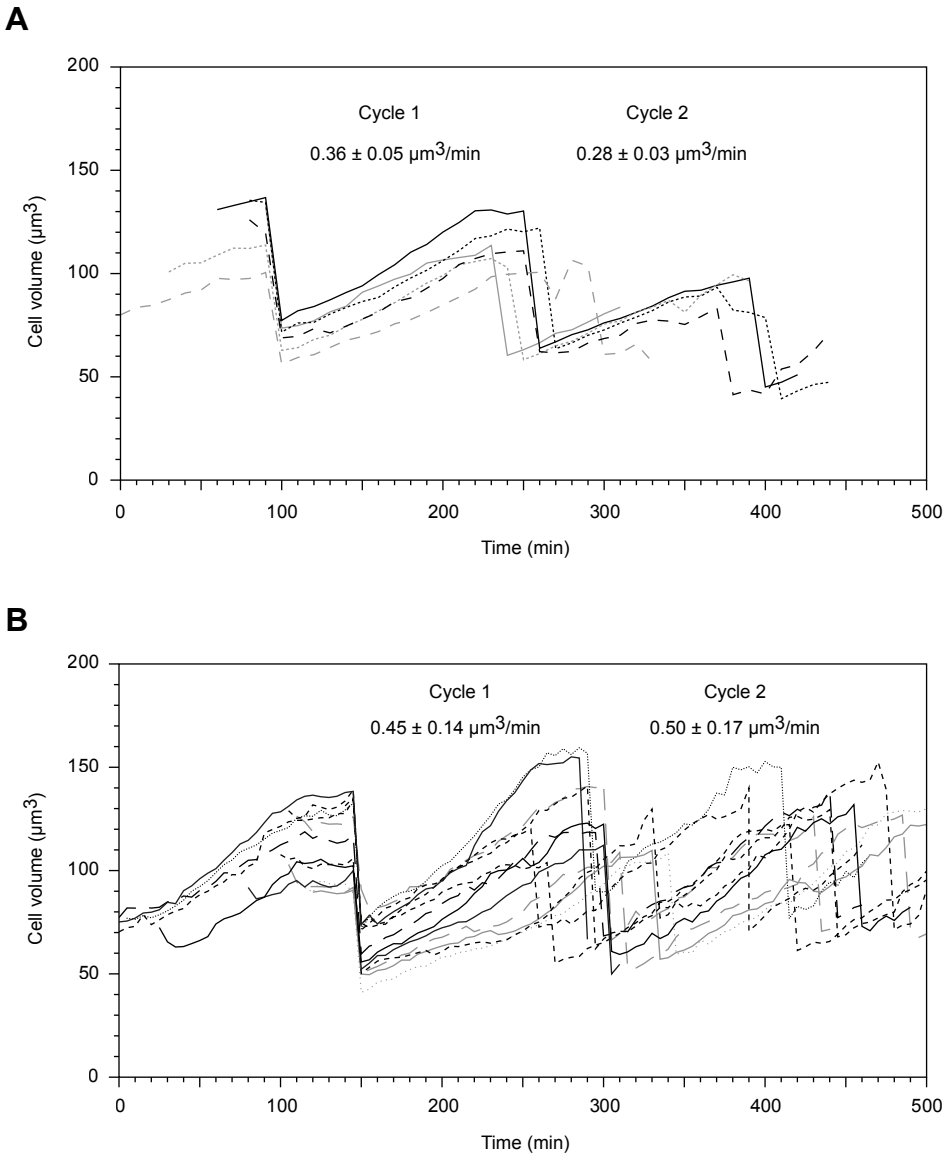
A
Cycle 1
0.36 ± 0.05 μm3/min
Cycle 2
0.28 ± 0.03 μm3/min
Cell volume (μm3)
Time (min)
B
Cycle 1
0.45 ± 0.14 μm3/min
Cycle 2
0.50 ± 0.17 μm3/min
Cell volume (μm3)
Time (min)